Physics of the Earth and Planetary Interiors 240 (2015) 132–141

Contents lists available at ScienceDirect

Physics of the Earth and Planetary Interiors

journal homepage: www.elsevier.com/locate/pepi

Seismological implications of a lithospheric low seismic velocity zone in Mars

Yingcai Zheng [a,b,c,*], Francis Nimmo [b], Thorne Lay [b]

[a] Department of Earth and Atmospheric Sciences, University of Houston, TX 77204, USA
[b] Department of Earth and Planetary Sciences, University of California Santa Cruz, Santa Cruz, CA 95064, USA
[c] Earth Resources Laboratory, Massachusetts Institute of Technology, Cambridge, MA 02139, USA

ARTICLE INFO

Article history:
Received 24 July 2014
Received in revised form 6 October 2014
Accepted 7 October 2014
Available online 18 October 2014

Keywords:
Mars
Planetary seismology
Mars seismological structure
Seismic low velocity zone

ABSTRACT

Most seismological models for the interior of Mars lack an upper mantle low velocity zone. However, there is expected to be a large thermal gradient across the stagnant conductive lid (lithosphere) of Mars. This gradient should tend to decrease elastic wave velocities with increasing depth, with this effect dominating the opposing tendency caused by increasing pressure with depth because Mars has low gravity. An upper mantle lithosphere with a low velocity zone (LVZ) beneath a thin high velocity "seismic lid" is thus predicted. The upcoming NASA InSight mission includes a three-component seismometer, which should provide the first opportunity to directly detect any lithospheric LVZ in Mars. Seismic wavefields expected for Mars mantle velocity structures with or without a strong LVZ are very distinct. The LVZ models predict shadow zones for high-frequency seismic body wave phases such as *P*, *S*, *PP* and *SS*, etc. The most diagnostic waves that can be used to evaluate presence of a lithospheric LVZ given a single seismometer are intermediate-period global surface waves, which travel along the great circle from a seismic source to the seismometer. An LVZ produces distinctive dispersion, with a Rayleigh wave Airy phase around 100 s period and very different surface wave seismograms compared to a model with no LVZ. Even a single observation of long-period surface waves from a known range can be diagnostic of the lithospheric structure. Establishing the existence of an LVZ has major implications for thermal evolution, volatile content and internal dynamics of the planet.

1. Introduction

The seismological low-velocity zone (LVZ) in Earth's upper mantle, first proposed by Gutenberg (1948, 1959), is closely linked to plate tectonics because it is related to thermal, volatile and compositional effects associated with the rheological transition from the lithosphere to the asthenosphere (e.g., Anderson, 1989; Stixrude and Lithgow-Bertelloni, 2005). An LVZ is simply a region from which the seismic velocity increases in both the upwards and downwards directions. Thermal modeling suggests the possible existence of a similar seismic LVZ within the lithosphere of Mars (Mocquet and Menvielle, 2000; Rivoldini et al., 2011; Nimmo and Faul, 2013). This Martian LVZ would be different than Earth's, being most pronounced within the thermal boundary layer rather than near its deepest levels. Establishing whether Mars has such an LVZ has important implications for our understanding of the internal dynamics, volatile content and thermal evolution of the Martian mantle.

In 2016, NASA's InSight (Interior exploration using Seismic investigations, geodesy and heat transport) Martian lander will deploy a single 3-component seismometer and a heat flow probe to study the planet's deep interior (Banerdt et al., 2013). Hopefully the seismic instrument will couple well to the surface and record broadband signals from sufficiently energetic sources that excite broadband seismic wavefields. In anticipation of this seismic data collection proving successful and high quality broadband recordings being obtained, we consider whether the presence of a lithospheric LVZ should have significant manifestations in the seismic wavefield that would allow its detection from a single sensor and (likely) sparse sources at various ranges. Many seismic models have been proposed for Mars (Fig. 1a) and most do not include an upper mantle LVZ (e.g., Okal and Anderson, 1978; Franck and Kowalle, 1994; Sohl and Spohn, 1997; Zharkov and Gudkova, 2005; Khan and Connolly, 2008; Walzer et al., 2010). Notable exceptions are those of Mocquet and Menvielle (2000) and Nimmo and Faul (2013).

* Corresponding author at: Department of Earth and Atmospheric Sciences, University of Houston, TX 77204, USA. Tel.: +1 7137436513.
E-mail addresses: yczheng@mit.edu, yzheng12@uh.edu (Y. Zheng).

http://dx.doi.org/10.1016/j.pepi.2014.10.004
0031-9201/

The case for the existence of an LVZ within Mars is straightforward. If a stagnant conductive thermal boundary layer, or "thermal lid" overlies a convective mantle (Toksöz and Hsui, 1978; Ogawa and Yanagisawa, 2011), a large temperature gradient will develop across the lithosphere (as is true for Earth's thermal boundary layer). Unlike for Earth, the thermal effect, which tends to reduce seismic velocity with increasing depth in the lithosphere, can overcome the competing effect of increasing pressure due to the low gravity of Mars (Nimmo and Faul, 2013). This results in a net decrease in seismic velocity with increasing depth within the thermal boundary layer. The magnitude of velocity reduction in the LVZ is a function of the temperature gradient in the stagnant lithosphere, which depends on the mantle potential temperature and the thermal lid thickness. Seismic velocity models based on the temperature profile adopted by Bertka and Fei (1997) do not result in an LVZ. This is because the temperature drop across the top 250 km of the lithosphere in that profile is only about 300 K, much less than expected for a stagnant lid (e.g., Ogawa and Yanagisawa, 2011). Mocquet and Menvielle (2000) assumed the presence of a thick stagnant lid and predicted an LVZ at a depth of 200–400 km; some of the models displayed in Rivoldini et al. (2011) also have an LVZ for a hot mantle (potential temperature > 1800 K). Nimmo and Faul (2013) also predicted the presence of an LVZ, though their main intent was to match the bulk tidal and dissipative properties of Mars. Although Verhoeven et al. (2005) considered a stagnant-lid convection scenario, their lid was too thick (it extends to 400–550 km depth) to result in a large thermal gradient with a prominent LVZ. None of these papers considered the detailed seismological implications of an LVZ.

The NASA InSight mission will provide an important opportunity to test the existence of a Martian lithospheric LVZ, if suitable seismic signals from as yet unknown sources are recorded. It is not our intent here to carry out a detailed investigation of whether such sources are likely to exist, nor to evaluate all possible causes of wavefield complexity such as 3D structure and anisotropy. Rather, in the rest of this paper we present seismic wavefields computed for end-member global velocity models for Mars with and without a lithospheric LVZ, guided by the model of Nimmo and Faul (2013). Consideration of the computed seismic wavefields identifies diagnostic attributes that can be sought for different epicentral ranges when long-period ground motion recordings for Martian sources are obtained.

2. Seismological models for Mars

Planetary seismological models prescribe the compressional (P-wave) velocity, V_P, shear (S-wave) velocity, V_S, density, and anelastic absorption factors, Q_P and Q_S for P- and S-waves, respectively, as functions of depth. At present, there are no constraints on seismic anisotropy for Mars, so usually isotropic models are considered.

The model we adopt is based on that described in Nimmo and Faul (2013). This model matches the observed bulk density and moment of inertia of Mars; it also satisfies the measured k_2 Love number and the tidal dissipation factor Q inferred from observation of Phobos' orbit. This model is simplified compared with other models in which detailed mineralogical and equation of state data are employed (e.g., Gudkova and Zharkov, 2004; Khan and Connolly, 2008; Rivoldini et al., 2011). However, compared with the enormous uncertainties in key parameters (such as the radius of the Martian core, and the bulk composition of the mantle), the approximations involved in our simple model are unlikely to matter. Furthermore, what we are primarily concerned with here is *differences* between models with and without a LVZ; such differences will not be very sensitive to changes in the background model parameters.

Below we describe the main aspects of the velocity model in more detail. We assume that Mars has differentiated into three compositionally distinct layers: the core, the mantle and the crust. We also assume Mars is spherically symmetric.

2.1. Crust

The Martian surface is characterized by a clear topographic dichotomy, the heavily-cratered southern highlands and relatively smooth northern lowlands with far fewer craters. The Martian crust is non-uniform, as shown by inverting the gravity and topography data from the Mars Global Surveyor (MGS) mission (Zuber, 2001). In general, the crust progressively thins from the southern pole to the northern pole. For our crustal model, we use the mean value of the crustal thickness, 50 km, and V_P = 6.0 km/s, V_S = 3.5 km/s, density = 2900 kg/m^3 (Zuber et al., 2000). We set shear Q to be $Q_S = 600$ and $Q_P = 9/4Q_S$.

2.2. Core

The Love number k_2 inferred from solar tides indicates the existence of at least an outer liquid core (Yoder et al., 2003). Whether Mars has a solid inner-core or not is uncertain. Existence of a solid inner core will have significant effect on seismic normal mode frequencies (Okal and Anderson, 1978). In our model, we do not include a solid inner core. A range of core radii is permitted when modeling the tidal k_2 and moment of inertia (Yoder et al., 2003); we adopt a baseline value of 1650 km similar to that employed by Nimmo and Faul (2013). To study the mantle LVZ, the exact radius is not critical. We assume 10^9 for the bulk Q in the fluid core, which means essentially no dissipation.

Because Nimmo and Faul (2013) were concerned primarily with dissipation in the mantle, they did not calculate seismic velocities in the core. In Appendix A we outline the procedure by which the core density and velocity structure were obtained.

2.3. Mantle

Derivation of the mantle seismic velocity and Q structure is described in detail in Nimmo and Faul (2013) and only a brief summary is given here. The anelastic properties of the mantle are based on experiments on Fo90 olivine conducted by Jackson and Faul (2010). To account for the fact that Mars is more iron-rich than the Earth (Longhi et al., 1992; Table 2 in Robinson and Taylor, 2001), we treat the reference density of our mantle material as a free parameter, constrained by the moment of inertia and bulk density of Mars. Iron enrichment will only increase the magnitude of any seismic LVZ (Mocquet et al., 1996). The temperature of the deep mantle is constrained by observations of Phobos' orbital decay, which yields the bulk k_2/Q ratio (see Bills et al., 2005), where Q is the tidal dissipation factor at the synodic period of Phobos (~11.106 h). Higher mantle temperatures and smaller grain sizes result in lower values of Q. Using an extended Burgers model, the seismic velocity and local Q near a seismic frequency of ~1.0 Hz can be derived for a specified temperature profile, and a bulk tidal Q and k_2 obtained for comparison with observations. The mantle potential temperature is inferred to be 1625 ± 75 K (Nimmo and Faul, 2013) for a stagnant thermal lid thickness of 150 km, in good agreement with some recent petrological studies based on remote-sensing observations (Baratoux et al., 2011; Baratoux et al., 2013). Solid phase changes, olivine-wadsleyite (Earth's 410-km discontinuity) and wadsleyite-ringwoodite (Earth's 520-km discontinuity) occur at Martian depths of around 1100 and 1400 km, respectively. The precise depths of these discontinuities, if obtained by seismological means in the future, could act as Martian internal absolute temperature tie-points. The third phase change, ringwoodite-perovskite (or the

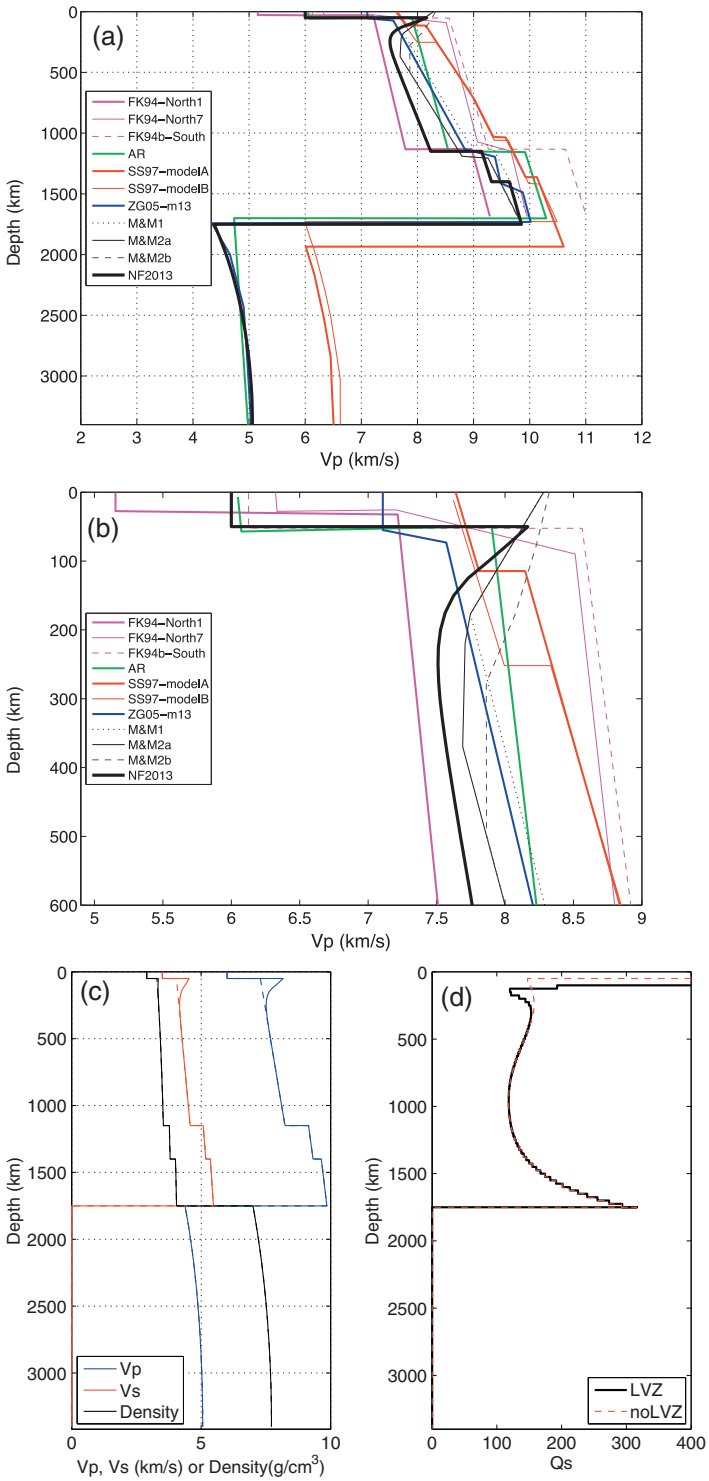

Fig. 1. (a) Representative Martian seismological models (*Vp*) showing no LVZs: FK94-North1, -North7, -South (Franck and Kowalle, 1994), AR (Okal and Anderson, 1978), SS97-model A&B (Sohl and Spohn, 1997); and models with LVZs: M&M1, 2a, 2b (Mocquet and Menvielle, 2000), and model NF2013 (Nimmo and Faul, 2013). (b) Zoomed-in for the upper 600 km of modes in (a); (c) Seismic velocities: *Vp* (blue), V_S (red), and density (black) for LVZ model (solid lines) and for noLVZ model (dash lines). Olivine phase transitions are included and give mantle discontinuities. (d) Q_S at 1.0 Hz for the LVZ model and noLVZ model. Tabulated model parameters for LVZ and noLVZ are in Table S1 and S2 in the supplementary online materials. (For interpretation of the references to colour in this figure legend, the reader is referred to the web version of this article.)

Earth's 660-km discontinuity) may or may not be present in Mars, depending on the core size and the temperature in the lowermost part of the mantle.

Because tidal dissipation depends primarily on shear and not bulk modulus, Nimmo and Faul (2013) did not present an explicit method for calculating *Vp*. To calculate *Vp* below we take the mantle bulk modulus $K_m = 2G_m(1 + \nu)/3(1–2\nu)$ where G_m is the (depth-dependent) shear modulus obtained by Nimmo and Faul (2013) and ν is the Poisson's ratio, taken to be 0.278 which results in $V_P/V_S = 1.8$ throughout the mantle. We also tested the Poisson's

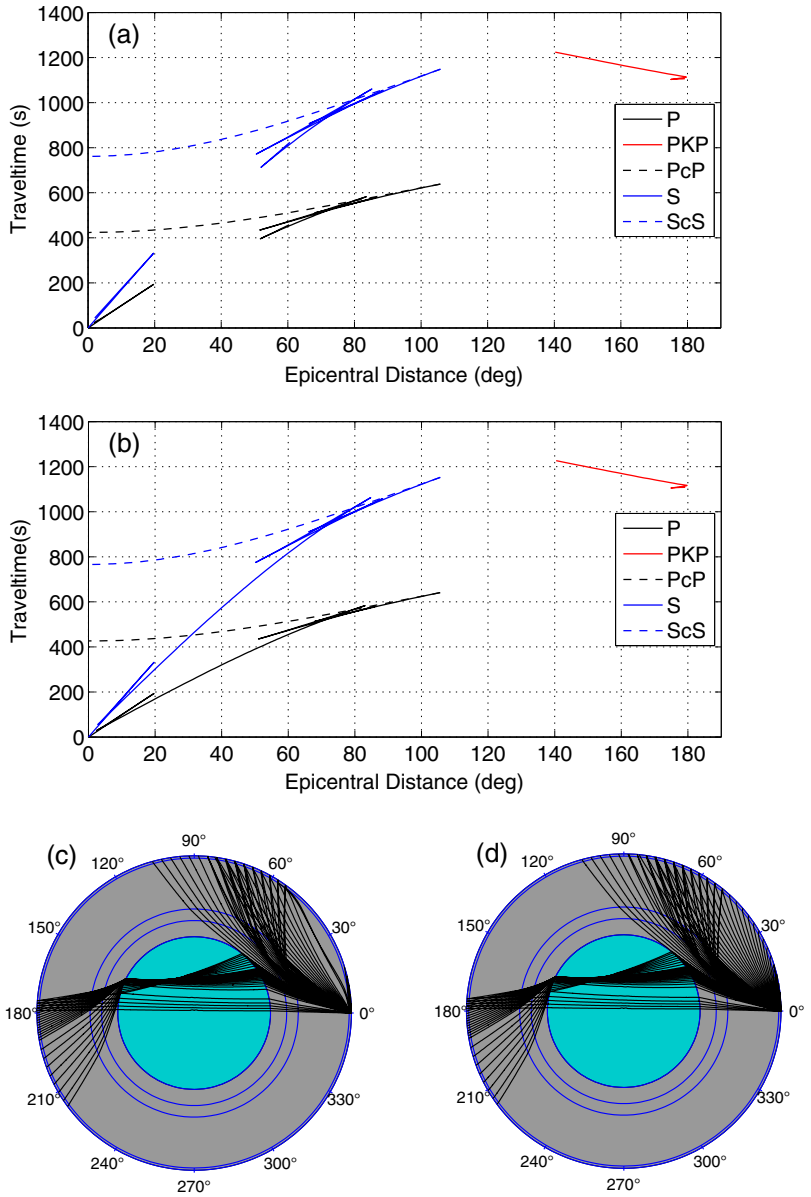

Fig. 2. Traveltime curves for LVZ (a) and noLVZ (b). Notice the direct P shadow in the range of 20–44° caused by the LVZ (a); and seismic rays for direct P (in the mantle) and PKP (through the core) phases for the LVZ (c) and noLVZ (d) models.

ratio $v = 0.25$ and the essential diagnostics for the LVZ remain unaffected. Details of Poisson's ratio and anisotropy will only be useful to address when bountiful seismic observations are obtained.

As discussed above, the main control on whether an LVZ exists is the near-surface temperature gradient. A common feature of previous thermal models (Fig. 1b) is that when the thermal gradient is large in the lid, an LVZ exists, and vice versa. For the nominal temperature profile described in Nimmo and Faul (2013), Fig. 1c shows calculated elastic wave speeds and densities. The Q_S model is shown in Fig. 1d, with Q_P assumed to be 9/4 Q_S.

The strong temperature increase within the stagnant thermal lid decreases seismic velocities with increasing depth in the upper mantle down to a depth of about 200 km, producing a thin "seismic lid" above a broad low velocity zone. To evaluate the seismological manifestations of this LVZ model, we produce a similar model with the same structure at all depths below 300 km, but with no seismic lid and a positive velocity increase with depth from the crust-mantle boundary, similar to earlier Martian models. We label the latter model the noLVZ model, recognizing that it is likely less justifiable on physical grounds than the LVZ model. Comparison of seismic wave computations for the LVZ and noLVZ models isolates the effects of the thin seismic lid and the waveguide structure of the associated LVZ in the lithosphere to establish the diagnostic wavefield characteristics, and makes uncertainties in the deep structure relatively unimportant. Given the predicted ground motions, we will then assess whether it is realistic to establish presence of an LVZ using just one 3-component seismometer.

An important potential caveat for single-station seismology is that if the Martian interior is as scattering as the lunar interior, surface waves may not be clearly recorded. However, the Moon and Mars are very different bodies – particularly in terms of near-surface water content and gravity – so the lunar experience does not provide much guidance in terms of what seismic waves can be measured and should be expected. Direct evidence from the early Viking experiment showed that the one possible recorded seismogram was more Earth-like than Moon-like (see Anderson

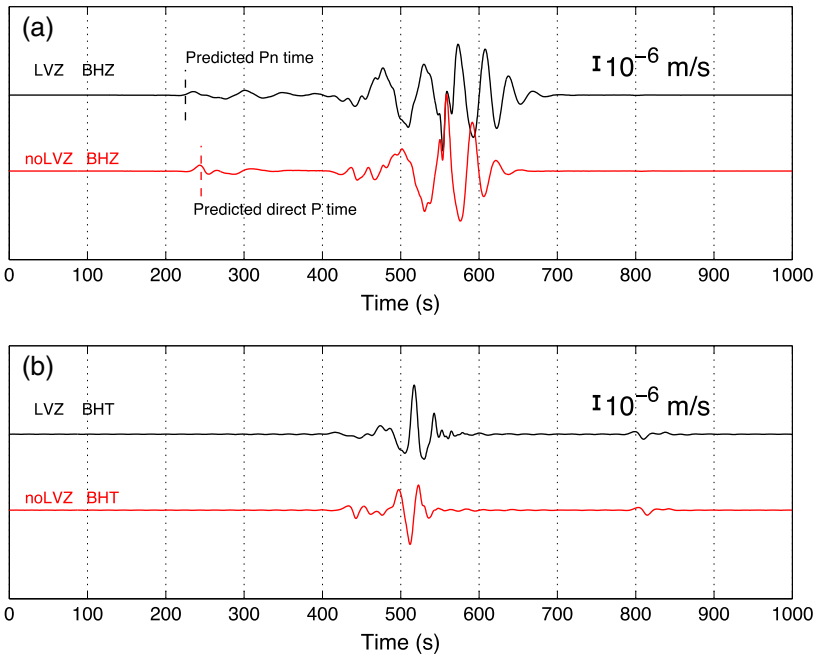

Fig. 3. (a) Vertical (BHZ) and (b) tangential (BHT) components of velocity seismograms at epicentral distance of 30°, bandpass-filtered between 200 and 25 s, for LVZ and noLVZ models. The seismic moment is 10^{18} Nm. The marsquake is a thrust event on a fault plane with strike 45°, dip 45° and rake 90°. The seismic moment is 10^{18} Nm. The epicenter is at (0°E, 0°N) and the source depth is 10 km. The receiver is located at (30°E, 0°N). Pn is the diffracted wave along the crust-mantle boundary.

et al., 1977). Indirect evidence from geophysics indicates that the lunar interior and the Martian interior should be different seismologically. Seismic scattering is caused by heterogeneities. The lunar crust is very heterogeneous (and fractured) but not dissipative so that high-frequency seismic waves reverberate for a very long time without much attenuation. The Martian crust is likely heterogeneous (though less fractured), but is expected to be more dissipative for high-frequency seismic waves. Fractures generated by impacts on Mars should be relatively compacted due to the larger gravity and presence of near-surface water. The lunar mantle might be more heterogeneous than the Martian mantle because of lower temperatures and lack of mantle convection (Laneuville et al., 2013). Given these contrasting differences between the Moon and Mars, it is useful to design and test some single-station seismological methodologies before the martian seismic data are returned. On the other hand, while there have been major advances in seismic instrumentation since the Apollo program, questions remain about how well a broadband seismometer deployed on the martian surface will resolve weak long-period motions.

3. Seismological signature of a lithospheric LVZ

Seismological studies of the Martian interior will require seismic sources producing sufficient elastic wave energy and high quality broadband seismometers. It is not clear what types or numbers of seismic sources exist on Mars. As reviewed by Lognonne and Johnson (2007), possible sources include potential marsquakes due to brittle faulting (Golombek et al., 1992; Knapmeyer et al., 2006; Taylor et al., 2013), asteroid impacts (Teanby and Wookey, 2011; Daubar et al., 2013), tidal loading, landslides, atmospheric hum, Chandler wobble, etc. (Solomon et al., 1991). During the 19 months of operation of the short-period seismometer on the Viking 2 lander, only atmospheric noise and maybe one marsquake were recorded (Anderson et al., 1977). Better ground coupling, sensitivity, and broad frequency range may allow us to observe signals from other types of sources. In this paper, we assume that an energetic source will occur and can be recorded by the broadband seismometer with good signal-to-noise for periods from 1 to 150 s.

For the LVZ and noLVZ models, we computed seismic wave attributes by a suite of methods, including conventional ray theory (Cerveny, 2005), normal mode theory (Aki and Richards, 1980; Woodhouse, 1988) and frequency-wavenumber (or angular order, in spherical coordinates) integration methods (Fuchs and Muller, 1971; Geller and Ohminato, 1994). We will not go into details about the methods as they are well established, and we confirmed compatibility of calculations for the various methods for specific sources and epicentral distances. To calculate the mode frequencies, we used the MINEOS code (Masters et al., 2011) and benchmarked its full waveforms with the Direct Solution Method (DSM) (Geller and Ohminato, 1994; Takeuchi et al., 1996). The normal mode method first searches for eigenfrequencies and their associated eigenfunctions and then expands the source force function onto those eigenfunctions to find the source excitation terms. Searching for the eigenfrequencies can be time consuming at high frequency as adjacent eigenfrequencies can be very close to each other. Normal modes are used to synthesize low-frequency (shortest period of ~16 s) seismograms. The DSM does not depend on root searching and can compute high frequency waves. Here we focus on the resulting wavefield characteristics.

3.1. Body waves

For a shallow seismic source in the crust (here we use 0 km depth), the most distinct signature of the LVZ model relative to noLVZ is the shadow zone for direct P (or S) wave (Fig. 2a and c) spanning the epicentral distance range of 20° to 55° (Fig. 2b and d). Gutenberg discovered Earth's LVZ by modeling the direct-wave amplitudes at different epicentral distances for which seismic rays traverse the LVZ (Gutenberg, 1959), but he had the advantage of having sources at intermediate depths within subducting slabs, which will not be present in the stagnant Martian lid. The shadow zone appears obvious, but in practice, diffraction along the crust-mantle boundary complicates the interpretation. Multiple sources at a wide range of epicentral distances could allow some confidence in the detection of the shadow zone, but full-waveform

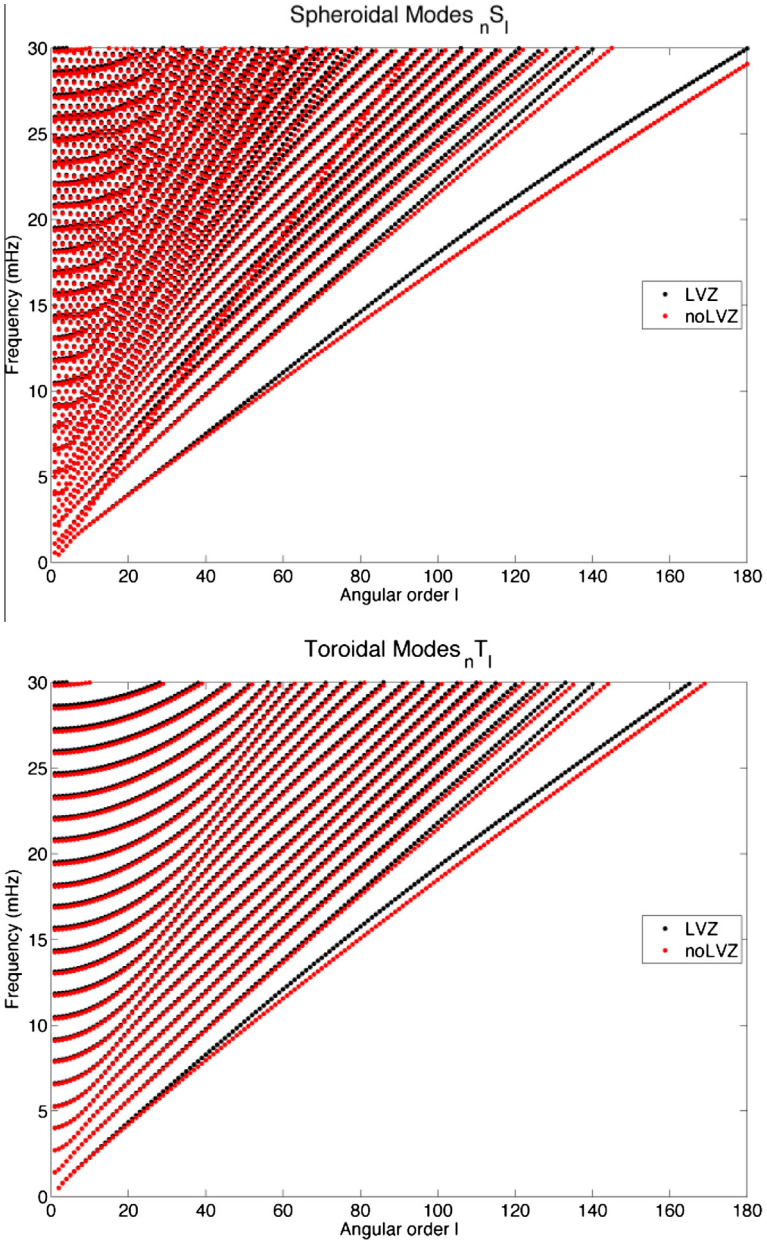

Fig. 4. Spheroidal (top) and toroidal (bottom) mode eigenfrequencies for LVZ and noLVZ models.

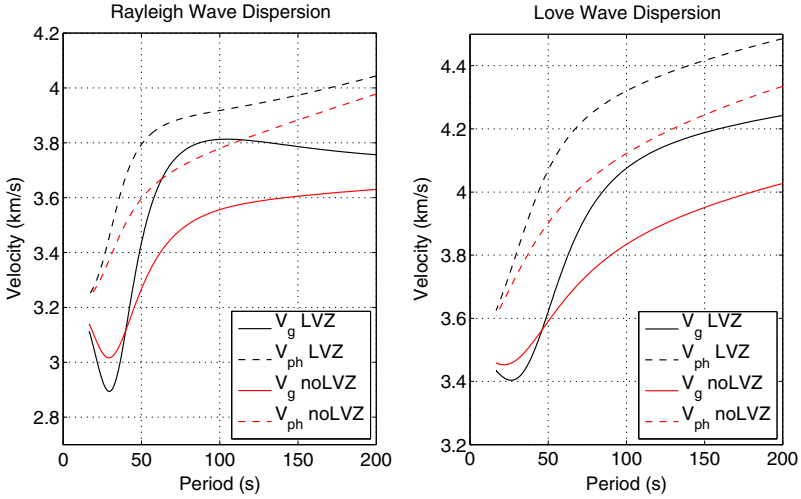

Fig. 5. Dispersion curves of phase (*V*ph) and group (*V*g) velocities for fundamental Rayleigh and Love modes for the LVZ and noLVZ models.

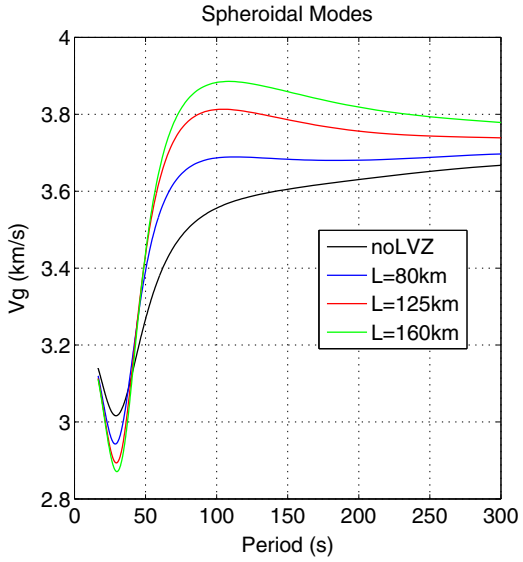

Fig. 6. Fundamental-mode Rayleigh-wave group velocities for Martian seismic velocity models with different lid thicknesses, *L*.

computation for the LVZ and noLVZ models indicates that the presence of a LVZ causes little identifiable difference in *long-period body* waves (Fig. 3). While frequency dependence of the waveforms might resolve the nature of the diffracted energy that fills the seismic shadow, it is likely this will not be viable if only a few sources are available.

3.2. Normal modes

Normal modes probe Mars as an entire planet (e.g., Gudkova and Zharkov, 2004), which is attractive given a small number of sensors, but challenging for resolving a localized upper mantle structural feature. Normal-mode seismology analyzes the vibrational eigenfrequencies of a planet (or the Sun in helioseismology) for a long recording of ground motion, assuming there is a sufficient single or continuous source of excitation. A single station may suffice for this purpose. If the gravest normal modes (e.g., angular order < 10) of Mars can be excited and identified, they can reveal whether the core is liquid or solid (Okal and Anderson, 1978). The period of, ${}_0S_2$, the longest period mode, is 2260 s for the LVZ model. For the noLVZ model, the period of ${}_0S_2$ is 2267 s. If the core is solid, this period can be much shorter (around 1000 s, depending on the structure), thus for the purpose of detecting the LVZ, the low frequency mode frequencies will not be diagnostic. For low angular orders less than 10, the frequency shifts due to an LVZ are very small for spheroidal, toroidal and radial modes (Fig. 4). However, frequency shifts are significant for large ℓ for fundamental modes and overtones. Identification of the modes for a single seismometer will be challenging and constrained by the source distribution and characteristics. However, it is possible to measure surface wave dispersion for those modes using a single seismometer.

3.3. Surface waves

Dispersion of intermediate period (30–150 s) mantle Rayleigh or Love waves is likely to be the most diagnostic observable for the existence of the LVZ (Fig. 5). For Rayleigh waves, there is a pronounced Airy phase (minima or maxima in the group velocity curve) around a period of 100 s, for the LVZ model, along with

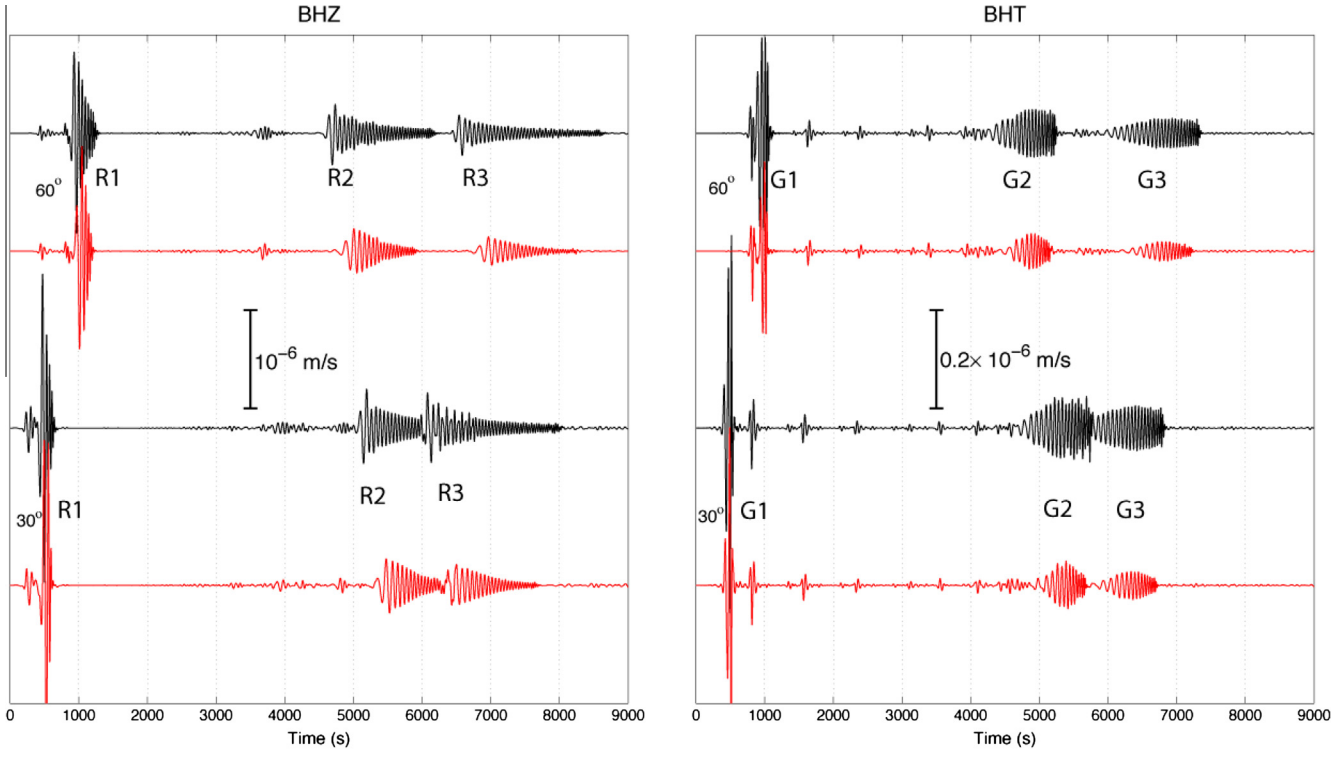

Fig. 7. Globally traversing Rayleigh (BHZ component; left) and Love (BHT component; right) waves for LVZ (black) and noLVZ (red) models at three different distances. The waveforms are bandpass filtered between 200 and 50 s using a Butterworth filter with two passes and two poles. The marsquake is a thrust event on a fault plane with strike 45°, dip 45° and rake 90°. The seismic moment is 10^{18} Nm. The epicenter is at (0°E, 0°N) and the source depth is 10 km. The receivers are located at (30°E, 0°N) and (60°E, 0°N). (For interpretation of the references to colour in this figure legend, the reader is referred to the web version of this article.)

significant overall shifts to higher phase and group velocities due to the presence of the seismic lid. For the noLVZ model, the Rayleigh wave group velocity increases monotonically beyond the crustal Airy phase located around 30 s. For different lid thicknesses (80 km and 160 km), Rayleigh wave dispersion curves are different (Fig. 6), with thicker lids giving faster group velocities and shifting the Airy phase to longer periods. The differences in dispersion give cumulative waveform differences that are substantial. Fig. 7 compares Rayleigh and Love waveforms at distances of 30° and 60° from a double-couple shear dislocation at a depth of 10 km for the LVZ and noLVZ models and large time-domain differences in Rayleigh waves are due to the mantle Airy phase. The maximum in the group-velocity dispersion was also recognized by Panning et al. (2006) as a way of probing Europa's ice shell structure. Assuming that an event's approximate location can be deduced from relative times of body wave arrivals and signal polarization information (with identification of the great-circle path based on separation of Love and Rayleigh motions or body wave polarizations), it should be possible to evaluate the dispersion in either time or frequency domain to test the likelihood of LVZ existence. Given a single seismometer and a large energy source somewhere on the planet, global-circling surface Rayleigh waves, R1, R2, R3, ... Rn (likewise, G1, G2, G3, ... Gn for Love waves) can be used to deduce the global average dispersion curves with high fidelity (Satô, 1958, p. 381 in Aki and Richards, 1980; Panning et al., 2012) provided the polar phase shift is taken into account (Brune et al., 1961) (see Figs. S1–S3 for single-station based dispersion measurement at different epicentral distances). With the specification of the InSight seismometer, it is estimated that about 20 events may have enough energy to excite global surface waves over the operational period of 720 days (Lognonne et al., 2012). Taylor et al. (2013) estimated a high likelihood of having tens of M_w 5.0 events in the Cerberus Fossae region per Earth's year. For the seismic event in Fig. 3, our calculations show that R1-R5 Rayleigh waves are above the instrument sensitivity and projected Martian wind noise (Lognonne et al., 2012). If this is the case, we would be able to determine the existence of the LVZ using a single seismometer if high signal-to-noise broadband recordings are recovered. There is no question that complexities such as radial anisotropy and 3D crustal and lithospheric structure can complicate the waveforms and possibly overwhelm the diagnostic differences we propose for simple 1D models. Even for the Earth, there is difficulty in resolving LVZ attributes with sparse data sets, so we do not want to be overly optimistic, but everything hinges on the uncertain nature of the data and sources that will be observed.

4. Conclusions

The possible existence of a pronounced seismic low velocity zone (LVZ) in the uppermost mantle of Mars is indicated because of the increased importance of thermal relative to pressure effects on velocity in the lithosphere of this low-gravity planet. Thermal models consistent with convection simulations and the inferred tidal Q of Mars predict a thin seismic lid below the crust-mantle boundary, with a pronounced LVZ extending several hundred kilometers across the thermal lithosphere. Based on seismological modeling for the resulting Mars seismic velocity structure, we find that the strongest indication of the presence of a lithospheric LVZ will be provided by dispersion characteristics of Rayleigh waves. This is due to the development of long-period Airy phases for structures with an LVZ. Single station observations of long-period dispersion for events that are approximately located should be viable as long as the sources are large enough to give good signal-to-noise ratio long-period surface wave observations. The broadband three-component seismometer to be deployed by NASA's InSight mission in 2016 may provide an opportunity to verify the existence of an LVZ in the Martian upper mantle. Doing so will provide valuable information for constraining Martian internal thermal evolution, volatile content and dynamics.

Acknowledgments

We are extremely grateful to Editor Professor Cormier for handling our paper and to two anonymous reviewers for their professional and careful reviews that greatly enhance the readability of the paper. During the course of this research, Professors Nafi Toksoz and Maria Zuber shared their scientific experiences, views, and insights about Mars and planetary seismology in general. Y.Z. also thanks Mike Fehler for his constant support and encouragement at MIT. T. Lay was supported by the United States NSF grant EAR-1245717. Y.Z. also thanks ERL/MIT for facilities support to carry out first part of this work. Financial support for publication comes from University of Houston.

Appendix A.

Below we outline a prescription for calculating the sound-speed inside the core (assumed liquid). This approach is significantly simplified compared with some other work (e.g., Gudkova and Zharkov, 2004; Khan and Connolly, 2008; Rivoldini et al., 2011). Our rationale for a simplified approach is twofold. First, the errors introduced by our approach are very small compared to major uncertainties in the bulk structure of Mars (such as the core radius). Second, we are focusing here primarily on the role of the mantle LVZ, so that our core velocity structure is of only secondary interest.

The pressure at the base of the mantle P_{cmb} is given by (e.g., Nimmo and Faul, 2013)

$$P_{cmb} = \frac{4}{3}\pi G \rho_m \left[R_c^3 \Delta\rho \left(\frac{1}{R_c} - \frac{1}{R} \right) + \frac{\rho_m}{2} \left(R^2 - R_c^2 \right) \right]$$

Here R_c is the core radius, ρ_m is the mantle density, $\Delta\rho$ is the core-mantle density contrast, R is the planetary radius, and G is the gravitational constant. This expression is approximate because it assumes a constant mantle density (constrained by the bulk density and moment of inertia of Mars). The errors introduced by this approximation are a few percent, very small compared to other uncertainties regarding the bulk structure of Mars (see Nimmo and Faul, 2013). The pressure at a radial position r within the core is then given by

$$P(r) = P_{cmb} + \frac{2}{3}\pi G \rho_c^2 \left(R_c^2 - r^2 \right)$$

A constant core density ρ_c is assumed here (constrained by the bulk density and moment of inertia). Again, the error introduced by this approximation is small compared to other uncertainties, especially because the pressure (and thus density) change across the Martian core is modest. In calculating the velocity profile within the core, we do allow the density to vary (see below). The temperature profile within the core $T(r)$ is assumed to be adiabatic:

$$T(r) = T_{cmb} \exp\left(\frac{R_c^2 - r^2}{D^2} \right)$$

where T_{cmb} is the temperature at the core-mantle boundary and D is a length scale given by (e.g., Labrosse et al., 2001)

$$D = \left(\frac{3C_p}{2\pi\alpha G \rho_c} \right)^{1/2}$$

where α is the thermal expansivity and C_p is the specific heat capacity (both assumed constant). We take the bulk modulus at

the core-mantle boundary (CMB) to be K_c. The bulk modulus inside the core is then calculated using a linear approximation (because the changes in T and P are small):

$$K_c(r) = K_c + (P(r) - P_{cmb})\frac{dK_c}{dP} + (T(r) - T_{cmb})\frac{dK_c}{dT}$$

Similarly, taking the density at the CMB to be ρ_c, the variation of density inside the core is calculated using

$$\rho(r) = \rho_c\left(1 + \frac{P(r) - P_{cmb}}{K_c}\right)(1 - \alpha[T(r) - T_{cmb}])$$

The P-wave velocity is then simply given by $V_p(r) = [K_c(r)/\rho(r)]^{1/2}$.

The core properties were obtained from the FeS end-member of Bertka and Fei (1998) and the compilation of Williams and Nimmo (2004). The value of Kc was derived from the one-bar value of 54 GPa and dK_c/dP. The value of T_{cmb} assumed is not critical, because the temperature contrast across the core matters much more than the absolute temperature. Mantle and bulk properties are from the reference model described in Nimmo and Faul (2013).

Table A1. Quantities used in construction of core velocity model. References are: (1) Nimmo and Faul (2013); (2) Bertka and Fei (1998); (3) Williams and Nimmo (2004).

Quantity	Value	Units	References	Quantity	Value	Units	References
R_c	1650	km	–	ρ_c	7000	kg m^{-3}	1
K_c	134	GPa	See text	dK_c/dP	4	–	2
dK_c/dT	−0.02	GPa K^{-1}	2	C_p	780	J kg^{-1} K^{-1}	3
T_{cmb}	2500	K	3	α	5.85×10^{-55}	K^{-1}	3
ρ_m	3526	kg m^{-3}	1				

Appendix B. Supplementary data

Supplementary data associated with this article can be found, in the online version, at http://dx.doi.org/10.1016/j.pepi.2014.10.004.

References

Aki, K., Richards, P.G., 1980. Quantitative Seismology. Freeman and Co., San Francisco.

Anderson, D.L., 1989. Theory of the Earth. Blackwell Scientific Publications, Boston.

Anderson, D.L., Miller, W.F., Latham, G.V., Nakamura, Y., Toksöz, M.N., Dainty, A.M., Duennebier, F.K., Lazarewicz, A.R., Kovach, R.L., Knight, T.C.D., 1977. Seismology on Mars. J. Geophys. Res. 82 (28), 4524–4546.

Banerdt, W.B., Smrekar, S., Hurst, K., Lognonne, P., Spohn, T., Asmar, S., Banfield, D., Boschi, L., Christensen, U., Dehant, V., Folkner, W., Giardini, D., Goetz, W., Golombek, M., Grott, M., Hudson, T., Johnson, C., Kargl, G., Kobayashi, N., Maki, J., Mimoun, D., Mocquet, A., Morgan, P., Panning, M., Pike, W.T., Tromp, J., van Zoest, T., Weber, R., Wieczorek, M., 2013. InSight: a discovery mission to explore the interior of Mars. Lunar Planet. Sci. Conf. 44, 1915.

Baratoux, D., Toplis, M.J., Monnereau, M., Gasnault, O., 2011. Therm**al history of Mars inferred from orbital geochemistry of volcanic provinces (vol 472, pg 338, 2011). Nature 475 (7355), 254.

Baratoux, D., Toplis, M.J., Monnereau, M., Sautter, V., 2013. The petrological expression of early Mars volcanism. J. Geophys. Res. Planets 118 (1). http://dx.doi.org/10.1029/2012JE004234.

Bertka, C.M., Fei, Y., 1997. Mineralogy of the Martian interior up to core-mantle boundary pressures. J. Geophys. Res. Solid Earth 102 (B3), 5251–5264.

Bertka, C.M., Fei, Y.W., 1998. Density profile of an SNC model Martian interior and the moment-of-inertia factor of Mars. Earth Planet. Sci. Lett. 157 (1–2), 79–88.

Bills, B.G., Neumann, G.A., Smith, D.E., Zuber, M.T., 2005. Improved estimate of tidal dissipation within Mars from MOLA observations of the shadow of Phobos. J. Geophys. Res. Planets 110 (E7).

Brune, J.N., Nafe, J.E., Alsop, L.E., 1961. The polar phase shift of surface waves on a sphere. Bull. Seismol. Soc. Am. 51 (2), 247–257.

Cerveny, V., 2005. Seismic Ray Theory, Cambridge University Press, Cambridge, UK, p. 724.

Daubar, I.J., McEwen, A.S., Byrne, S., Kennedy, M.R., Ivanov, B., 2013. The current martian cratering rate. Icarus 225 (1), 506–516.

Franck, S., Kowalle, G., 1994. Seismic velocity models for an internally asymmetric Mars. Earth Moon Planets 65 (3), 277–290.

Fuchs, K., Muller, G., 1971. Computation of synthetic seismograms with the reflectivity method and comparison with observations. Geophys. J. Int. 23 (4), 417–433.

Geller, R.J., Ohminato, T., 1994. Computation of synthetic seismograms and their partial derivatives for heterogeneous media with arbitrary natural boundary-conditions using the direct solution method. Geophys. J. Int. 116 (2), 421–446.

Golombek, M.P., Banerdt, W.B., Tanaka, K.L., Tralli, D.M., 1992. A prediction of Mars seismicity from surface faulting. Science 258 (5084), 979–981.

Gudkova, T.V., Zharkov, V.N., 2004. Mars: interior structure and excitation of free oscillations. Phys. Earth Planet. Inter. 142 (1–2), 1–22.

Gutenberg, B., 1948. On the layer of relatively low wave velocity at a depth of about 80 kilometers. Bull. Seismol. Soc. Am. 38 (2), 121–148.

Gutenberg, B., 1959. Physics of the Earth's Interior. Springer, New York.

Jackson, I., Faul, U.H., 2010. Grainsize-sensitive viscoelastic relaxation in olivine: towards a robust laboratory-based model for seismological application. Phys. Earth Planet. Inter. 183 (1–2), 151–163.

Khan, A., Connolly, J.A.D., 2008. Constraining the composition and thermal state of Mars from inversion of geophysical data. J. Geophys. Res. Planets 113 (E7).

Knapmeyer, M., Oberst, J., Hauber, E., Wahlisch, M., Deuchler, C., Wagner, R., 2006. Working models for spatial distribution and level of Mars' seismicity. J. Geophys. Res. Planets 111 (E11).

Labrosse, S., Poirier, J.P., Le Mouel, J.L., 2001. The age of the inner core. Earth Planet. Sci. Lett. 190 (3–4), 111–123.

Laneuville, M., Wieczorek, M.A., Breuer, D., Tosi, N., 2013. Asymmetric thermal evolution of the Moon. J. Geophys. Res. Planets 118 (7), 1435–1452.

Lognonne, P., Banerdt, W.B., Hurst, K., Mimoun, D., Garcia, R., Lefeuvre, M., Gagnepain-Beyneix, J., Wiezorek, M., Mocquet, A., Panning, M., Beucler, E., Deraucourt, S., Giardini, D., Boschi, L., Christensen, U., Goetz, W., Pike, T., Johnson, C., Weber, R., Larmat, K., Kobayashi, N., Tromp, J., 2012. InSight and single-station broadband seismology; from signal and noise to interior structure determination. Lunar Planet. Sci. Conf. 43, 1983.

Lognonne, P., Johnson, C., 2007. Planetary seismology. In: Treatise on Geophysics. Elsevier, Amsterdam, pp. 69–122.

Longhi, J., Knittle, E., Holloway, J.R., Wanke, H., 1992. The bulk composition, mineralogy and internal structure of Mars. In: Kieffer, H.H., et al. (Eds.), In Mars, Univ. Arizona Press, Tucson, pp. 184–208.

Masters, G., Barmine, M., Kientz, S., 2011. Mineos (version 1.0.2), Computational Infrastructure for Geodynamics (CIG), <http://www.geodynamics.org> (last accessed 2.10.2014).

Mocquet, A., Menvielle, M., 2000. Complementarity of seismological and electromagnetic sounding methods for constraining the structure of the Martian mantle. Planet Space Sci. 48 (12–14), 1249–1260.

Mocquet, A., Vacher, P., Grasset, O., Sotin, C., 1996. Theoretical seismic models of Mars: the importance of the iron content of the mantle. Planet Space Sci. 44 (11), 1251–1268.

Nimmo, F., Faul, U.H., 2013. Dissipation at tidal and seismic frequencies in a melt-free, anhydrous Mars. J. Geophys. Res. Planets 118, 2558–2569.

Ogawa, M., Yanagisawa, T., 2011. Numerical models of Martian mantle evolution induced by magmatism and solid-state convection beneath stagnant lithosphere. J. Geophys. Res. Planets 116 (E8), E08008.

Okal, E.A., Anderson, D.L., 1978. Theoretical models for Mars and their seismic properties. Icarus 33, 514–528.

Panning, M., Lekic, V., Manga, M., Cammarano, F., Romanowicz, B., 2006. Long-period seismology on Europa: 2. Predicted seismic response. J. Geophys. Res. Planets 111 (E12), E12008.

Panning, M.P., Mocquet, A., Beucler, E., Banerdt, W.B., Lognonne, P., Boschi, L., Johnson, C., Weber, R.C., Anonymous, 2012. InSight; using Earth data to demonstrate inversion techniques for Mars' interior, Abstracts of Papers Submitted to the Lunar and Planetary Science Conference, 43, 0-Abstract 1515.

Rivoldini, A., Van Hoolst, T., Verhoeven, O., Mocquet, A., Dehant, V., 2011. Geodesy constraints on the interior structure and composition of Mars. Icarus 213 (2), 451–472.

Robinson, M.S., Taylor, G.J., 2001. Ferrous oxide in Mercury's crust and mantle. Meteorit. Planet. Sci. 36 (6), 841–847.

Satô, Y., 1958. Attenuation, dispersion, and the wave guide of the G wave. Bull. Seismol. Soc. Am. 48 (3), 231–251.
Sohl, F., Spohn, T., 1997. The interior structure of Mars: Implications from SNC meteorites. J. Geophys. Res. Planets 102 (E1), 1613–1635.
Solomon, S.C., Anderson, D.L., Banerdt, W.B., Butler, R.G., Davis, P.M., Duennebier, F.K., Nakamura, Y., Okal, E.A., Phillips, R.J., 1991. Scientific Rationale and Requirements for a Global Seismic Networks on Mars, LPI Tech. Rpt, 91–02, Lunar and Planetary Institute, Houston, p. 51.
Stixrude, L., Lithgow-Bertelloni, C., 2005. Mineralogy and elasticity of the oceanic upper mantle: origin of the low-velocity zone. J. Geophys. Res. Solid Earth 110 (B3).
Takeuchi, N., Geller, R.J., Cummins, P.R., 1996. Highly accurate P-SV complete synthetic seismograms using modified DSM operators. Geophys. Res. Lett. 23 (10), 1175–1178.
Taylor, J., Teanby, N.A., Wookey, J., 2013. Estimates of seismic activity in the Cerberus Fossae region of Mars. J. Geophys. Res. Planets, n/a-n/a.
Teanby, N.A., Wookey, J., 2011. Seismic detection of meteorite impacts on Mars. Phys. Earth Planet. Inter. 186 (1–2), 70–80.
Toksöz, M.N., Hsui, A.T., 1978. Thermal history and evolution of Mars. Icarus 34 (3), 537–547.
Verhoeven, O., Rivoldini, A., Vacher, P., Mocquet, A., Choblet, G., Menvielle, M., Dehant, V., Van Hoolst, T., Sleewaegen, J., Barriot, J.P., Lognonne, P., 2005. Interior structure of terrestrial planets: Modeling Mars' mantle and its electromagnetic, geodetic, and seismic properties. J. Geophys. Res. Planets 110 (E4).
Walzer, U., Burghardt, T., Hendel, R., Kley, J., 2010. Towards a dynamical model of Mars' Evolution, pp. 485–510.
Williams, J.P., Nimmo, F., 2004. Thermal evolution of the Martian core: implications for an early dynamo. Geology 32 (2), 97–100.
Woodhouse, J., 1988. The calculations of eigenfrequencies and eigenfunctions of the free oscillations of the Earth and the Sun. In: Doornbos, D.J. (Ed.), Seismological Algorithms, Computational Methods and Computer Programs. Academic Press, London, UK, pp. 321–370.
Yoder, C.F., Konopliv, A.S., Yuan, D.N., Standish, E.M., Folkner, W.M., 2003. Fluid core size of mars from detection of the solar tide. Science 300 (5617), 299–303.
Zharkov, V.N., Gudkova, T.V., 2005. Construction of Martian interior model. Sol. Syst. Res. 39 (5), 343–373.
Zuber, M.T., 2001. The crust and mantle of Mars. Nature 412 (6843), 220–227.
Zuber, M.T., Solomon, S.C., Phillips, R.J., Smith, D.E., Tyler, G.L., Aharonson, O., Balmino, G., Banerdt, W.B., Head, J.W., Johnson, C.L., Lemoine, F.G., McGovern, P.J., Neumann, G.A., Rowlands, D.D., Zhong, S.J., 2000. Internal structure and early thermal evolution of Mars from Mars Global Surveyor topography and gravity. Science 287 (5459), 1788–1793.